Probing Energetics of Aβ Fibril Elongation by Molecular Dynamics Simulations

Takako Takeda and Dmitri K. Klimov*
Department of Bioinformatics and Computational Biology, George Mason University, Manassas, Virginia

ABSTRACT Using replica exchange molecular dynamics simulations and an all-atom implicit solvent model, we probed the energetics of $A\beta_{10-40}$ fibril growth. The analysis of the interactions between incoming Aβ peptides and the fibril led us to two conclusions. First, considerable variations in fibril binding propensities are observed along the Aβ sequence. The peptides in the fibril and those binding to its edge interact primarily through their N-termini. Therefore, the mutations affecting the Aβ positions 10–23 are expected to have the largest impact on fibril elongation compared with those occurring in the C-terminus and turn. Second, we performed weak perturbations of the binding free energy landscape by scanning partial deletions of side-chain interactions at various Aβ sequence positions. The results imply that strong side-chain interactions—in particular, hydrophobic contacts—impede fibril growth by favoring disordered docking of incoming peptides. Therefore, fibril elongation may be promoted by moderate reduction of Aβ hydrophobicity. The comparison with available experimental data is presented.

INTRODUCTION

A growing number of disorders, including Alzheimer's, Parkinson's, type II diabetes, and Creutzfeldt-Jakob disease, are attributed to aggregation and amyloid assembly of polypeptide chains (1). A complex cascade of structural transitions underlies amyloid assembly, which involves oligomerization of individual chains and formation of amyloid fibrils (2). Recent experimental data indicate that oligomers, in some cases as small as dimers (3), appear to be the primary cytotoxic species (4–6). Even though amyloid fibrils by themselves appear to be relatively inert species with respect to neuron cells, they play an important role as reservoirs of monomers, which are in dynamic equilibrium with soluble oligomeric species (7–9). In addition, amyloid fibrils appear to be covered with disordered layer of polypeptides, which may also induce cytotoxicity (10). The internal organization of amyloid fibrils is remarkably homogeneous due to the formation of extensive β-sheet structure (11–15). Backbone hydrogen bonds (HBs) and hydrophobic contacts lend significant stability to amyloid fibrils against thermal, chemical, or mechanical denaturations (16).

Amyloid assembly of Aβ peptides is linked to the onset of Alzheimer's disease. These peptides are released after proteolysis of amyloid precursor protein in a variety of lengths, of which 40-mer $A\beta_{1-40}$ is the most abundant. Recently, the structure of the $A\beta_{1-40}$ fibril protofilament has been derived from solid-state nuclear magnetic resonance experiments (13) (Fig. 1 *a*). This structure reveals parallel in-registry β-sheets formed by Aβ peptides (12,14). However, elucidation of the mechanisms of fibril formation and growth remains a formidable challenge (17,18). Preformed Aβ fibrils appear to serve as templates for the deposition of Aβ monomers (17,19). Furthermore, Aβ fibril elongation was proposed to proceed via two-stage dock-lock mechanism (20–22). The first stage involves docking of disordered Aβ monomer to the fibril without its integration into the fibril structure. The second stage locks a monomer in the fibril state through structural reorganization of bound peptides.

Despite the progress in experimental observations of fibril growth, its description on a molecular level is incomplete. Recent bioinformatics approaches were successful in predicting the amyloidogenic propensities of polypeptide chains by taking into account hydrophobicity, net charges, secondary structure propensities, and residue patterns (23,24). Computer simulations have the important advantage of providing molecular-level details of fibril elongation for specific peptides (25). For example, all-atom molecular dynamics (MD) simulations of peptide fragments of various lengths support the elongation mechanism with multiple dock-lock stages (26–31).

In our recent studies, we have probed the thermodynamics and free energy landscape of Aβ fibril growth (30,31). Here we continue our in silico investigation of fibril elongation by focusing on the interactions involved in the deposition of Aβ peptides on the edges of preformed fibrils. The specific questions addressed in this study are as follows:

1. What are the interactions and regions in Aβ peptides that drive their binding to the growing fibril edge?
2. Is it possible to identify binding-prone locations in Aβ fibril, which are most frequently involved in the interactions with incoming peptides?
3. What are the contribution of side-chain interactions to fibril elongation and their potential interplay with backbone hydrogen bonding?

In general, experiments show that the structural transitions in wild-type Aβ peptides related to their binding to

Submitted January 6, 2009, and accepted for publication March 3, 2009.

*Correspondence: dklimov@gmu.edu

Editor: Ruth Nussinov.

0006-3495/09/06/4428/10 $2.00

doi: 10.1016/j.bpj.2009.03.015

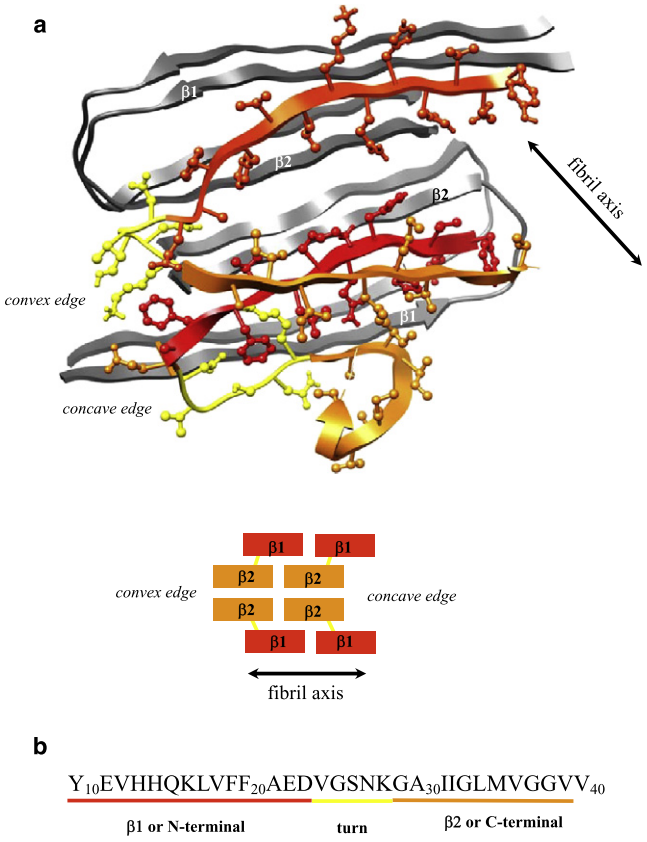

FIGURE 1 (*a*) Cartoon representation of the $A\beta_{10–40}$ hexamer. Four Aβ peptides in backbone representation (in *gray*, online) form a fibril fragment. Two incoming peptides with side chains shown (in *color*, online) are bound to the fibril edge. The fibril protofilament consists of four laminated, in-registry β-sheets formed by the β1 and β2 strands in an Aβ sequence. The N-termini (in *red*, online) of incoming peptides form parallel off-registry β-sheets with the fibril N- and C-termini (i.e., the locked state; see Methods for details). The C-termini (in *orange*, online) of incoming peptides form few interactions with the fibril. The stagger of inner β2 sheets with respect to β1 results in the appearance of two distinct fibril edges—concave and convex. On the concave edge, indented β2 sheets form a groove. The fibril structure is derived from nuclear magnetic resonance measurements (13) and visualized using Chimera (61). (*b*) The sequence of $A\beta_{10–40}$ monomer and the allocation of the β1 and β2 fibril β-strands (also referred to as N- and C-termini) and the turn.

or unbinding from the fibril are extremely slow, spanning the timescales from 1 s to 10^3 min (21,22,32). Therefore, explicit solvent MD simulations at a constant temperature are unlikely to provide any reliable sampling. Consequently, to answer the questions posed above, we employ all-atom implicit solvent protein model and replica exchange molecular dynamics (REMD) (33). Extensive sampling in a wide range of temperatures allowed us to compute the distributions of side-chain contacts and HBs formed between Aβ peptides and amyloid fibrils. In addition, we use the free energy perturbation method to evaluate the contributions of individual Aβ side chains to the binding energetics.

METHODS

Molecular dynamics simulations

Simulations of Aβ peptides were performed using CHARMM MD program (34) and all-atom force field CHARMM19 coupled with the solvent accessible surface area implicit solvent model (35). A detailed description of this model, as well as the discussion of its applicability and testing, is given in Supporting Material.

In this work, we consider a hexamer system formed by $A\beta_{10–40}$ peptides, which are N-terminal truncated fragments of wild-type $A\beta_{1–40}$ (Fig. 1 *a*). Further description of the Aβ hexamer system is provided in Supporting Material and in our previous studies (30,31). Throughout the article, the peptides in gray in Fig. 1 *a* are referred to as fibrils, and the colored peptides are termed incoming, or edge, peptides.

Replica exchange simulations

To achieve exhaustive conformational sampling, we used REMD (33). This method has shown its efficiency in sampling rugged free energy landscapes and has been applied to study protein folding and aggregation (31,36–40). The details of REMD implementation are presented in Supporting Material and in our previous study (31). The error analysis for the fibril system and the convergence of REMD simulations were reported earlier (31).

Computation of structural probes

To probe the interactions between incoming peptide and the fibril, we computed the number of side-chain contacts. A side-chain contact was considered formed if the distance between the centers-of-mass of side chains is <6.5 Å (41). Backbone HBs between NH and CO groups were assigned according to Kabsch and Sander (42). In all, we defined two classes of backbone HBs between incoming peptides and the fibril. The first includes any peptide-fibril HB. The second class corresponds to parallel β-sheet HBs. A parallel HB (pHB) is formed between the residues i and j, if at least one other HB is also present between $i+2$ and j or $j+2$ (or between $i-2$ and j or $j-2$). For any HB we define a registry offset $R = |j-i|$, where j and i are the indices of the residues in the incoming and fibril peptides linked by HB. In-registry parallel alignment of peptides in the Aβ fibril displayed in Fig. 1 *a* corresponds to $R = 1$. In general, pHBs may result in arbitrary registry offset R. The bound states of incoming peptides with large number of pHBs are termed "locked" (Figs. 1 *a* and 2), whereas the states lacking pHBs are referred to as "docked" (31).

Throughout the article, angular brackets $\langle \ldots \rangle$ imply thermodynamic averages. Because hexamer system includes two indistinguishable incoming peptides, we report averages over two peptides. The distributions of states produced by REMD were analyzed using the multiple histogram method (43).

λ-Expansion analysis

The λ-expansion was initially proposed to evaluate the contribution of nonnative interactions to protein folding (44). In this approach, the density of states is computed using the protein system, which incorporates only native interactions. The nonnative interactions are then introduced as weak perturbations that allow one to use the native-only density of states. Thermodynamic functions can be recomputed using the multiple histogram method and the energy function with native and nonnative interactions.

Using a similar approach, we considered, as a perturbation, the deletion of the interactions formed by the side chain of the residue j in incoming peptides. The energy $E_{sc}(j)$ includes nonbonded van der Waals and electrostatic interactions formed by the side chain j as well as the contribution of the side chain to solvation energy. The energy $E_{sc}(j)$ accounts for the interactions formed by the side chain j in both incoming peptides. The new energy function is then defined as $E_{eff}^{m} = E_{eff}^{wt} - \lambda E_{sc}(j)$, where E_{eff}^{wt} is the effective energy of the unperturbed system. The adjustable parameter λ determines the extent to which the interactions formed by the side chain j are deleted.

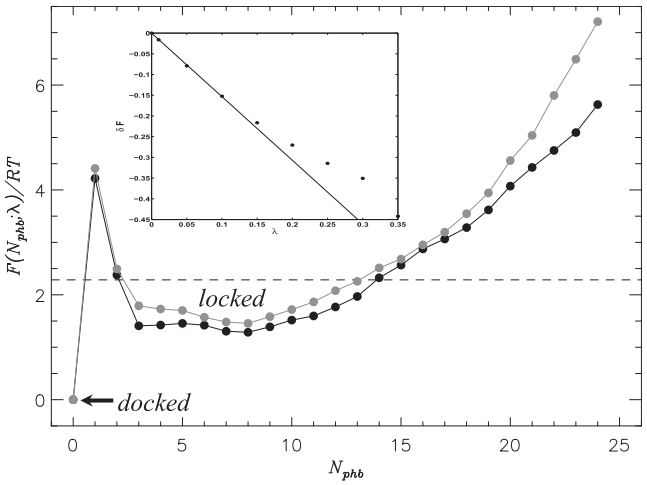

FIGURE 2 The free energy of incoming peptide $F(N_{\rm phb};\lambda)$ as a function of the number of peptide-fibril pHBs, $N_{\rm phb}$. The data for the wild-type ($\lambda = 0$) and the mutant, in which Phe^{19} side-chain interactions are partially deleted ($\lambda = 0.3$), are in shaded and solid representation, respectively. The docked and locked states are indicated. The energetic perturbation caused by partial deletion of Phe^{19} interactions stabilizes the locked state by ~35% (as measured by δF). The free energy level $F_{\rm L,\ min} + 1.0RT$ used in defining the mutant locked state is marked by the dashed line. The free energy of the docked state is set to zero. The inset shows the linear dependence of the change in free energy gap between docked and locked states $\delta F(\lambda)$ on small λ. The straight line represents linear fit.

If $\lambda = 0$, the original (i.e., wild-type) energy function is recovered, whereas $\lambda = 1$ corresponds to the mutant, in which the interactions formed by the side chain j are completely eliminated. We used λ-expansion to compute the free energy $F(N_{\rm phb};\lambda)$ as a function of the number of parallel peptide-fibril pHBs $N_{\rm phb}$ at various values of λ (see Supporting Material).

The impact of side-chain interactions was evaluated as follows. The free energy profile $F(N_{\rm phb};\lambda)$ reveals two free energy basins associated with the docked ($N_{\rm phb} = 0$) and locked states (Fig. 2) (31). The latter were operationally defined as the collection of states with the free energies in the interval ($F_{\rm L,\ min}$; $F_{\rm L,\ min} + 1.0RT$), where $F_{\rm L,\ min}$ is the free energy minimum at $N_{\rm phb} > 0$. The free energy gap between the locked and docked states (with the free energies $F_{\rm L}$ and $F_{\rm D}$) is $\Delta F_{\rm L-D} = F_{\rm L} - F_{\rm D}$. Partial ($0 < \lambda < 1$) deletion of the side chain j results in the change in free energy gap $\Delta\Delta F_{\rm L-D}(\lambda) = \Delta F_{\rm L-D}(\lambda) - \Delta F_{\rm L-D}(\lambda = 0)$. For small λ, one can write $\delta F(\lambda) \approx \lambda\partial(\delta F)/\partial\lambda|_{\lambda=0}$, where $\delta F(\lambda) = \Delta\Delta F_{\rm L-D}(\lambda)/|\Delta F_{\rm L-D}(\lambda = 0)|$. The contribution of the side chain j to the binding free energy is represented by the slope $\partial(\delta F)/\partial\lambda$, which can be obtained from fitting $\delta F(\lambda)$ with linear function (Fig. 2). Consistent with the assumption of small perturbations in free energy landscape due to mutation, $\delta F(\lambda)$ shows linear behavior up to $\lambda \lesssim 0.2$ for most residues.

RESULTS

Interactions between Aβ peptides and fibrils: maps of side-chain contacts and hydrogen bonds

As described in Methods, we have used REMD and all-atom implicit solvent model to compute thermally weighted distributions of interactions between Aβ_{10-40} peptides and amyloid fibrils (Fig. 1 *a*). We have previously reported that docking of Aβ peptides to amyloid fibrils is completed at the temperature $T_{\rm d} \approx 380$ K (31). At the lower (locking) temperature, $T_{\rm l} \approx 360$ K Aβ peptides adopt partially ordered parallel β-sheet conformations on the edges of amyloid fibrils. Other conformational states (including antiparallel β-sheets) have higher free energies at $T \leq T_{\rm l}$. Consequently, all thermodynamic quantities in this article are computed at $T_{\rm l}$. Before presenting the results, it is convenient to identify key sequence regions in Aβ peptides. Based on the allocation of β-structure in Aβ_{1-40} amyloid (13), we distinguish the N-terminus (residues 10–23, corresponding to the β-strand β1), the turn region (residues 24–28), and the C-terminus (residues 29–39, corresponding to the β-strand β2) (Fig. 1).

Fig. 3 *a* displays the thermal contact map $\langle C(i,j)\rangle$, which gives the probability of forming side-chain contact between fibril amino acid i and the amino acid j in incoming peptides. Although the probabilities $\langle C(i,j)\rangle$ are generally low (<0.35), several patterns in peptide-fibril interactions can be seen. First, the diagonal traces of contacts signify the formation of parallel and antiparallel β-sheets by incoming peptides (see below). It is also clear that parallel β-sheets involve either the N- or C-termini of the incoming peptides and the fibril, but rarely span the entire Aβ sequence. Second, Fig. 3 *a* suggests that, compared with other interactions, those between the C-termini of incoming and fibril peptides are suppressed. This finding is illustrated in Table S1 (available in Supporting Material), which contains the numbers of side-chain contacts between the C- and N-termini. Although these numbers are generally in excess of eight, there are only 3.3 contacts between the C-termini of incoming and fibril peptides.

To assess the distribution of interactions along Aβ sequence, we plot in Fig. 3 *b* the number of peptide-fibril side-chain contacts $\langle C_{\rm p}(j)\rangle$ formed by the residues j in incoming peptides. The profile $\langle C_{\rm p}(j)\rangle$ suggests that there is a preference for Aβ peptide to interact with the fibril via its N-terminus. Indeed, the total number of side-chain contacts formed by the N-terminus is 22.8 (1.6 per residue), whereas the C-terminus forms only 12.0 (1.1 per residue). Most residues in the incoming peptide form, on an average, fewer than two side-chain contacts with the fibril. The exception is Glu^{11}, which is engaged in approximately three contacts.

The thermal averages of the numbers of peptide-fibril side chain contacts $\langle C_{\rm f}(i)\rangle$ formed by the fibril residues i are presented in Fig. 3 *c*. Similar to $\langle C_{\rm p}(j)\rangle$ in Fig. 3 *b*, the N-terminus of the fibril forms, on an average, more peptide-fibril contacts than the C-terminus (the total numbers of contacts are 21.6 and 15.6, respectively, or 1.5 and 1.4 per residue). Although the profile of $\langle C_{\rm f}(i)\rangle$ is fairly smooth in the C-terminus, there are dramatic variations in $\langle C_{\rm f}(i)\rangle$ in the N-terminus. The odd-numbered residues form a larger number of side-chain contacts compared with their even-numbered counterparts. In the N-terminus, the side chains of odd-numbered residues are inward-pointing and are partially buried on the fibril edge, whereas the side chains of even-numbered residues are located on the fibril facet (30). Consequently, the alternating pattern in $\langle C_{\rm f}(i)\rangle$ is due to the strong preference of Aβ peptides to bind to the edges of the fibril rather than to its sides (31). It is also worth noting that there are few side-chain contacts

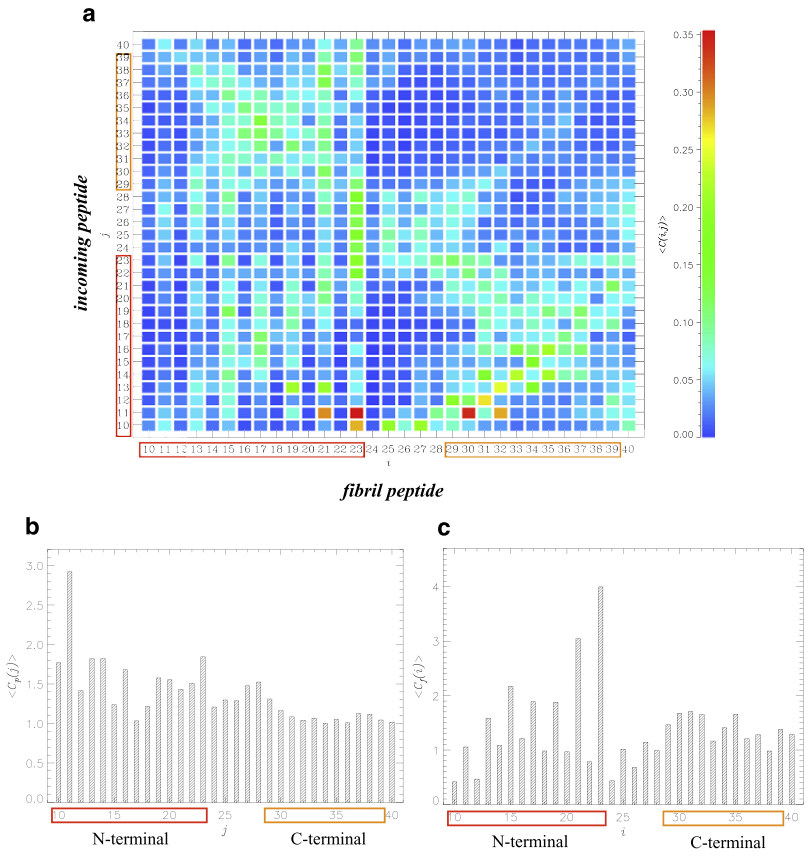

FIGURE 3 (*a*) The thermal contact map $\langle C(i, j)\rangle$ displays the probabilities of forming side-chain contacts between amino acids i from the Aβ fibril and j from incoming peptide. $\langle C(i, j)\rangle$ is color-coded according to the scale on the right. The map $\langle C(i, j)\rangle$ indicates that the contacts between Aβ C-termini are rare. (*b* and *c*) The distributions of contacts, $\langle C_p(j)\rangle$ and $\langle C_f(i)\rangle$, formed by the side chains in incoming and fibril peptides, respectively. Both plots show the preference for the N-terminus to form peptide-fibril interactions. The N- and C-terminal residues in this figure and in Figs. 4 and 5 are in boxes.

formed by the residues in the fibril turns. For example, the sum of $\langle C_f(i)\rangle$ for the fibril turn is only 4.3 contacts (0.9 per residue), which is smaller than the number of contacts in the C-terminus. In contrast, the turn regions of incoming peptides form the number of side-chain contacts with the fibril (6.8 contacts or 1.4 per residue) comparable to those formed by the C-terminus.

Parallel peptide-fibril HBs represent the basis for emerging locked states of Aβ peptides bound to the fibril (Fig. 1 *a*) (31). The thermal distribution of pHB $\langle N_{phb}(i, j)$ between fibril amino acid i and the amino acid j in incoming peptide is shown in Fig. 4 *a*. The distribution of $\langle N_{phb}(i, j)\rangle$ shows similarities with the contact map in Fig. 3 *a*. Most pHBs are formed either by N- or C-termini of the edge and fibril peptides, but very few occur between their C-termini. Specifically, Table S1 demonstrates that the average number of pHBs between the C-termini is only 0.3, which is significantly lower than the numbers of pHBs between other Aβ regions. Similar results are obtained for the distribution of all HBs formed between incoming peptides and the fibril.

We have previously shown that the edge Aβ peptides rarely form in-registry parallel β-sheets with the fibril (31). To quantify the alignment of incoming peptides with the fibril arising due to pHBs, we computed the average registry offsets $\langle R\rangle$. It follows from Table S2 that a typical offset for N- or C-terminal pairs is small ($\langle R\rangle \lesssim 3$). The minimal $\langle R\rangle$ is observed for the pHB occurring between the N-termini of the edge and fibril peptides (*lower-left corner* in Fig. 4 *a*). However, due to binding of N-(C-)terminus of incoming peptide to C-(N-) fibril terminus, the registry offset $\langle R\rangle$ may reach up to 17. Interestingly, the binding between the mixed pairs of termini still results in a small registry offset between the β-strands (Table S2).

Following the approach used for side-chain contacts we considered the number of peptide-fibril HBs $\langle N_{hb}{}^{p}(j)\rangle$ formed by the residues j in incoming peptides (Fig. 4 *b*). Despite some variations between residues (e.g., for Val[12], His[13]) the distribution $\langle N_{hb}{}^{p}(j)\rangle$ suggests that all regions of incoming Aβ peptide participate in the HBs with the fibril. This finding is confirmed by computing the total number of HBs formed by the N- and C-termini (4.6 and 4.5 HBs, respectively, or 0.3 and 0.4 per residue). Qualitatively similar results were obtained for the distribution of pHB (31). For reference, the total average numbers of HB and pHB between incoming peptide and the fibril are 10.5 and 6.0 at $T_1 = 360$ K (31).

The distribution of HBs in fibril peptides, $\langle N_{hb}{}^{f}(i)\rangle$ (Fig. 4 *c*), is qualitatively different from that in Fig. 4 *b*.

First, the total number of HBs formed by the fibril N-terminus (6.7 or 0.5 per residue) is considerably larger than that in the C-terminus (3.2 or 0.3 per residue). Similar observation has been made for the distribution of pHBs in the N- and C-termini (3.9 vs. 2.0, respectively).

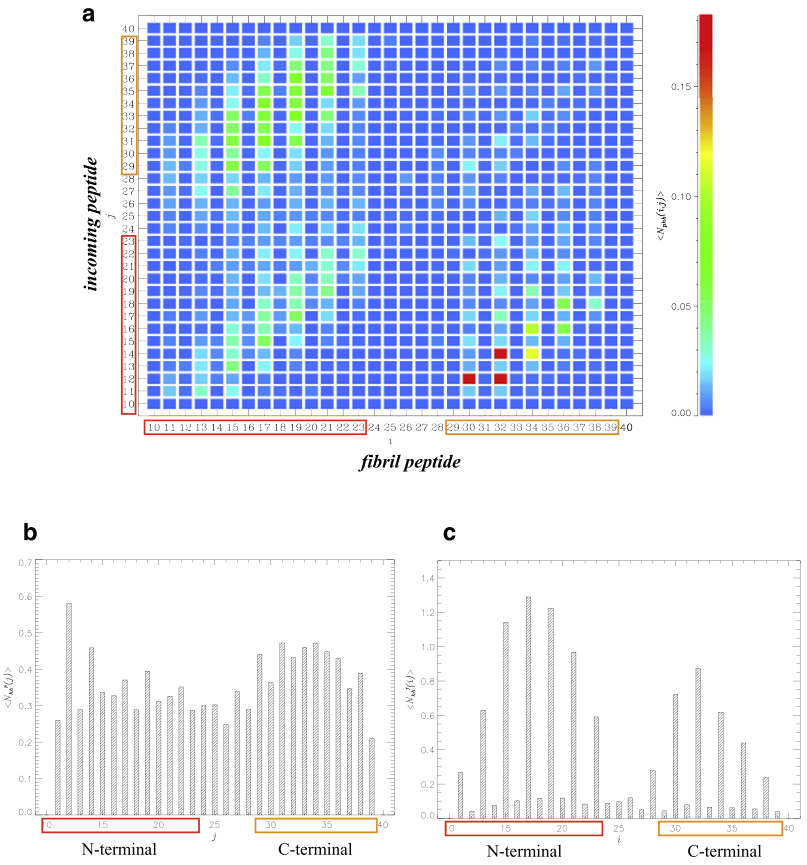

FIGURE 4 (*a*) The thermal pHB map $\langle N_{\mathrm{phb}}(i, j)\rangle$ displays the probabilities of forming parallel HBs between amino acids i from the Aβ fibril and j from incoming peptide. $\langle N_{\mathrm{phb}}(i, j)\rangle$ is color-coded according to the scale on the right. The plot shows that the elements of parallel β-sheets occur between the Aβ N- and C-termini, but very rarely between the two C-termini. (*b* and *c*) The distributions of HBs, $\langle N_{\mathrm{hb}}{}^{\mathrm{p}}(j)\rangle$ and $\langle N_{\mathrm{hb}}{}^{\mathrm{f}}(i)\rangle$, formed by the residues in incoming and fibril peptides, respectively. With some variations, all regions of incoming peptide form HBs with the fibril. In contrast, most peptide-fibril HBs are formed by the N-terminus of the fibril peptide.

Second, the sum of $\langle N_{\mathrm{hb}}{}^{\mathrm{f}}(i)\rangle$ for the turn region is only 0.6 or 0.1 per residue. Therefore, the turns in the fibril peptides form very few HBs with incoming peptides.

Third, Fig. 4 *c* reveals an alternating pattern in $\langle N_{\mathrm{hb}}{}^{\mathrm{f}}(i)\rangle$ distribution along Aβ sequence. This observation can be explained as follows. On the concave fibril edge, the donors and acceptors of odd-numbered residues in the N-terminus and even-numbered residues in the C-terminus are dangling and exposed to solvent (Fig. 1 *a*). Because the affinity of the concave edge with respect to incoming peptides is ~10 times stronger than that of the convex edge (31), the distribution $\langle N_{\mathrm{hb}}{}^{\mathrm{f}}(i)\rangle$ reflects the formation of peptide-fibril HBs available on the concave edge.

It is also of interest to compare the relative contributions to binding energetics of side-chain interactions and HBs. To this end, we normalized the number of peptide-fibril side-chain contacts $\langle C_{\mathrm{p}}(j)\rangle$ by the number of contacts $C_{\mathrm{p},\,0}(j)$ formed by the residue j in the edge peptide adopting experimental fibril structure. Similarly, we considered the ratio of $\langle N_{\mathrm{hb}}{}^{\mathrm{p}}(j)\rangle$ to the number of HBs $N_{\mathrm{hb},\,0}{}^{\mathrm{p}}(j)$ formed by the residue j in the edge peptide adopting experimental fibril structure. Fig. S2 shows the difference $B(j) = \langle C_{\mathrm{p}}(j)\rangle/C_{\mathrm{p},\,0}(j) - \langle N_{\mathrm{hb}}{}^{\mathrm{p}}(j)\rangle/N_{\mathrm{hb},\,0}{}^{\mathrm{p}}(j)$ as a function of sequence position j. Positive values of $B(j)$ in the N-terminus suggest that side chains provide most of the binding interactions for incoming Aβ peptides in this sequence region.

Taken together, the results presented above suggest a dominant contribution of the Aβ N-terminus to binding energetics. These observations are rationalized in Discussion.

Contribution of side-chain interactions to the binding free energy landscape

As described in Methods, we map the contribution of Aβ side chains to binding energetics by computing the slopes $\partial(\delta F(j))/\partial\lambda$ for all nonglycine residues j in incoming peptides. The distribution of $\partial(\delta F(j))/\partial\lambda$ in Fig. 5 *a* suggests several observations.

First, the slopes in the N-terminus, except for Glu[22], tend to have large and negative values ($-1.5 \lesssim \partial(\delta F)/\partial\lambda < 0$). In contrast, the slopes in the C-terminus and turn have considerably smaller values ($|\partial(\delta F)/\partial\lambda| < 0.5$) and alternating signs. This suggests that the contribution of Aβ side chains to peptide binding is highly uneven. Compared with the N-terminus, the turn and C-terminus have relatively minor impact on the binding free energy landscape.

Second, it is important to consider slope signs. Negative slopes imply that the free energy of the locked state decreases due to partial deletion of side-chain interactions. In other words, negative slopes implicate stabilization of the ordered locked state. As it follows from Fig. 5 *a*,

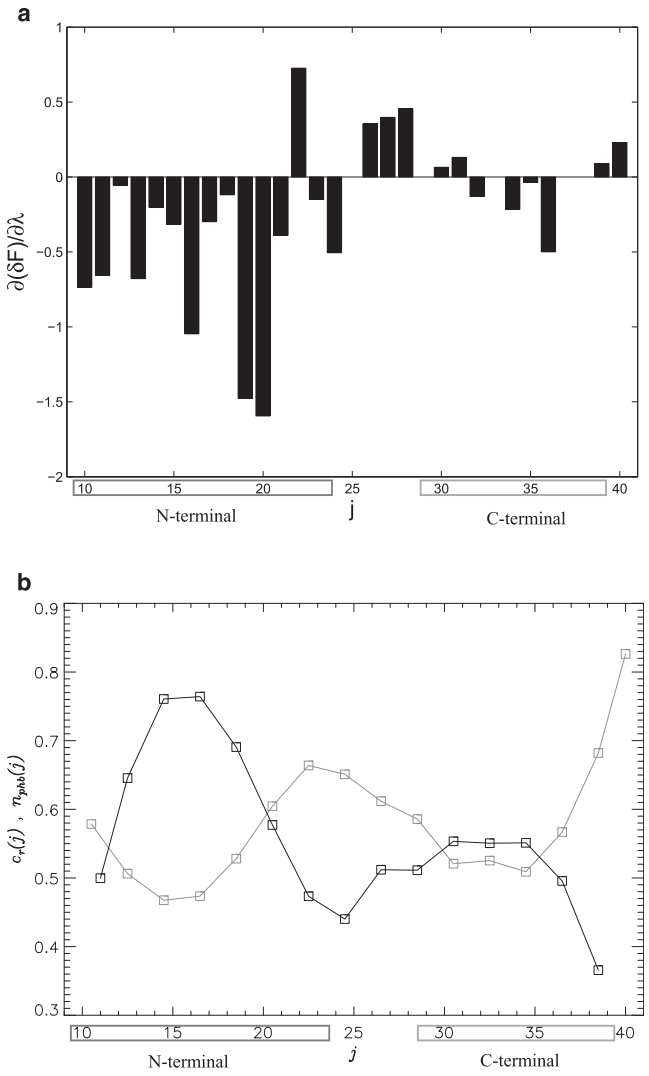

FIGURE 5 (*a*) Distribution of slopes $\partial(\delta F(j))/\partial\lambda$ along the sequence of incoming Aβ peptide. The slope $\partial(\delta F(j))/\partial\lambda$ characterizes the change in the binding free energy landscape arising in response to partial deletion of the interactions formed by the side chain *j*. The distribution of slopes suggests that almost all side-chain interactions in the N-terminus reduce the stability of the locked state. (*b*) The fractions of random contacts $c_r(j) = \langle C_r(j)\rangle/\langle C_p(j)\rangle$ (in *shading*) and pHBs $n_{phb}(j) = \langle N_{phb}{}^p(j)\rangle/\langle N_{hb}{}^p(j)\rangle$ (in *solid representation*) are plotted for residues *j* in incoming peptide. ($\langle C_r(j)\rangle$ and $\langle N_{phb}{}^p(j)\rangle$ are the thermal numbers of random side-chain contacts and pHB at *j*.) The plot indicates that $c_r(j)$ and $n_{phb}(j)$ are anticorrelated.

all side-chain interactions in the N-terminus (excluding Glu^{22}) reduce the thermodynamic stability of the locked state.

Third, it is interesting to note that negative slopes in the N-terminus are obtained for polar as well as nonpolar amino acids.

Fourth, the most significant changes in the binding free energy landscape result from partial elimination of side-chain interactions formed by Phe^{19} and Phe^{20} ($\partial(\delta F)/\partial\lambda \simeq -1.5$ in Fig. 5 *a*).

DISCUSSION

Binding propensity varies along the sequence of the Aβ peptide

We have previously shown that Aβ peptides bound to the edges of amyloid fibril adopt multiple docked and locked conformational states (31). The locked states differ from the rest by an elevated number of pHBs, which result in the formation of parallel β-sheets by incoming peptides on fibril edges. In this study, we showed that the parallel β-sheets formed by incoming peptides may have large registry offsets $\langle R\rangle \gtrsim 15$ (Table S2). This finding implies that these β-sheets may be completely off-registry and, therefore, be different from the in-registry parallel β-sheets in the fibril interior ($R = 1$). More importantly, we explored the distribution of binding interactions between incoming peptides and the fibril.

The analysis of the distributions of side-chain contacts and HBs suggests that fibril peptides form most of their interactions with incoming peptides using their N-termini (Figs. 3 *c* and 4 *c*). For example, the number of side-chain contacts formed by the fibril N-terminus is larger than that formed by the C-terminus by 40% (21.5 vs. 15.6). With respect to HBs, the difference exceeds the factor of 2 (6.7 vs. 3.2). The results further suggest that the fibril turn forms relatively few contacts and HBs with the incoming peptides. With respect to side-chain contacts, similar distribution of binding interactions applies to incoming peptides. For example, the number of side-chain contacts formed by the N-terminus of incoming peptide with the fibril is larger than that for the C-terminus by almost a factor of 2 (22.8 vs. 12.0, Fig. 3 *b*). This finding is strongly supported by the analysis of free energy perturbations caused by partial deletions of side chains in incoming peptides. Indeed, Fig. 5 *a* suggests that the largest side-chain contribution to the binding energetics comes from the N-terminus. However, the preferential engagement of the N-terminus is somewhat muted due to relatively uniform distribution of peptide-fibril HBs along the sequence of incoming peptide. For example, the C-terminus and the turn are involved in the interactions with the fibril to the same extent as the N-terminus (the numbers of HBs in the N- and C-termini are 4.6 and 4.5, respectively; see Fig. 4 *b*).

For fibril peptides, the importance of their N-terminus for binding can be rationalized, if one takes into account that the C-terminus is buried in the groove on the concave fibril edge and is less exposed to solvent than the N-terminus (Fig. 1 *a*) (13). In fact, in the experimental fibril structure, the solvent-accessible surface area per residue in the N-terminus is 93 $Å^2$, but it is only 30 $Å^2$ for the C-terminus. Because the concave edge has a significantly stronger binding affinity to incoming peptides than the convex edge (31,45), the structural features of the concave edge determine different affinities of the Aβ termini.

It is more challenging to explain the preference of the N-terminus of incoming peptide to engage in peptide-fibril interactions. This observation may be due to the flexibility

of the C-terminus imparted by the concentration of Gly residues (Fig. 1 *b*). Indeed, experiments and simulations have previously demonstrated that the structural fluctuations in the C-terminus of Aβ_{1-40} are significantly larger than in the N-terminus (46,47). Therefore, one may speculate that binding of the C-terminus involves higher entropic costs than those associated with the N-terminus. Interestingly, this conjecture is consistent with the recent experiments, which showed that the elimination of Gly residues in the Aβ sequence increases the rates of amyloid formation by depleting the population of oligomeric species (48). It is worth pointing out that, in our simulations, the least frequent interactions occur between the C-termini (Figs. 3 *a* and 4 *a* and Table S1). From the discussion above it appears that these interactions are disfavored because of the confluence of two factors—flexibility of C-termini and the presence of the groove on the concave edge.

A suggestion that Aβ C-terminus may not represent the primary aggregation interface was also put forward by Hou et al. (49), who measured the distribution of chemical shifts in Aβ_{1-40}, and by Melquiond et al. (50). Consistent with this proposal, the removal of the sequence fragment 14–23 from Aβ, which approximately coincides with the N-terminus in Aβ_{10-40}, prevents aggregation (51). On the other hand, the fragment Aβ_{1-28}, in which the C-terminus is truncated, retains amyloidogenic propensity (52). In the mutation screening of the entire Aβ sequence, half of mutations reducing amyloidogenic propensity involve the residues Leu^{17}, Val^{18}, and Phe^{19} from the N-terminus (53). Finally, in our earlier study, which used an EEF1 implicit solvent model, we also observed that, compared with the N-terminus, the Aβ C-terminus forms weak interactions with the fibril (30). These experimental and computational observations are consistent with our current finding that the N-terminus is critically important for fibril elongation.

It is interesting to compare our identification of the Aβ N-terminus as the most aggregation-prone region with bioinformatic predictions (23). Taking into account hydrophobicity, net charges, secondary structure propensities, and residue patterns, Pawar et al. (23) have predicted that the Aβ sequence contains two aggregation-prone regions, 15–21 and 30–40. The first region occurs in the N-terminus of Aβ_{10-40}, which is in agreement with our simulation data. However, the second region is in the C-terminus—at variance with our data suggesting that the C-terminus is less important for aggregation than the N-terminus. It is likely that the aggregation propensities (23) do not take into account the structural details of amyloid fibrils. Hence, the discrepancy is probably caused by the groove on the concave edge (Fig. 1 *a*), which apparently disfavors C-terminal binding.

Role of side-chain interactions in fibril elongation

We performed perturbations in the binding free energy landscape by partially deleting side-chain interactions formed by individual amino acids. As described earlier in Methods and in Results, the slope $\partial(\delta F(j))/\partial\lambda$ reflects the changes in the free energy of the locked state due to partial deletion of the side chain j.

The main result in Fig. 5 *a* is that all slopes in the aggregation-prone N-terminus (except for Glu^{22}) are negative. The slopes elsewhere in the Aβ sequence have alternating signs and smaller values. As explained in Results, negative slope $\partial(\delta F(j))/\partial\lambda$ implies that the deleted interactions formed by the side chain j destabilize the locked state. This result is somewhat surprising and requires further analysis. To this end, we decomposed side-chain contacts formed by incoming peptide into two categories—parallel and random contacts. The former are those contacts, which occur in close proximity to pHBs. Specifically, if a side-chain contact is formed by the amino acids, which also form pHB, or by their immediate neighbors (no more than one residue apart), such contact is classified as parallel. All other side-chain contacts are assumed random, because they do not participate in parallel β-sheet interactions. In Fig. 5 *b*, the fractions of random contacts $c_r(j)$ and pHBs $n_{phb}(j)$ are plotted. Consistent with Fig. 4 *a*, $n_{phb}(j)$ reaches maximum in the N- and C-termini and minimum within the turn (31). Interestingly, $c_r(j)$ demonstrates an anticorrelated behavior with respect to $n_{phb}(j)$. The overall correlation coefficient for these two quantities is -0.7 (-0.7 in the N-terminus and -0.6 in the C-terminus). Thus, Fig. 5 *b* suggests that random contacts destabilize pHB and, therefore, the associated locked state. On the contrary, random contacts are expected to stabilize docked states with few pHB. Because, on an average, random contacts constitute about two-thirds of all peptide-fibril contacts, partial deletion of side-chain interactions lends additional stability to pHBs and the locked state.

Fig. 5 *a* shows that both polar and hydrophobic side chains destabilize pHBs. However, by far, the largest impact on free energy landscape occurs upon partial deletion of aromatic Phe^{19} and Phe^{20}. This result is consistent with the importance of these residues for Aβ amyloidogenesis observed experimentally (53,54). The slope amplitudes in the C-terminus are significantly smaller than in the N-terminus. We have shown above that most side-chain peptide-fibril interactions are formed by the Aβ N-termini. It appears likely that the small slope values in the C-terminus are caused by the overall weakness of peptide-fibril interactions in this sequence region.

It is important to put our findings, concerning the role of side chains in binding energetics, in the context of other studies. Lu et al. have probed the formation of amyloidlike β-sheets for two peptides, polar β2m83-89 and hydrophobic Aβ_{16-22} (55). They found that hydrophobicity is inversely correlated with the stability of amyloid-competent β-sheet states, which are similar to our locked states. Their results are consistent with our observations on the role of side chains in Aβ binding.

Experimental data show that the decrease in hydrophobicity generally results in reduced amyloidogenic propensity

measured by aggregation rates or by the aggregation free energy (56,57). However, our data suggest the opposite trend: that partial deletion of side-chain interactions, including hydrophobic, stabilizes the locked amyloidlike state. We believe that careful analysis of experimental data allows us to reconcile apparently conflicting findings. First, experiments suggest that changes in hydrophobicity have the largest impact on nucleation time rather than on the time of fibril elongation (57). If the rate-limiting step in Aβ aggregation is the dimer assembly resulting from diffusive search (58), then one may expect that the reduced amyloidogenic propensity of less hydrophobic mutants observed experimentally is primarily the consequence of higher nucleation barrier for oligomerization. Because our simulations probe the postnucleation stage of fibril elongation, the impact of side-chain interactions may differ from that seen experimentally.

Second, Peim et al. have conducted a systematic experimental mutation scan at the position Val^{18} of $A\beta_{1-40}$ and obtained the respective free energies of fibrillation, ΔG_{fib} (59). In Fig. 6, we plot ΔG_{fib} for the most hydrophobic residues at the position 18 as a function of their Kyte-Doolittle hydrophobic score. Replacing Val^{18} with Ile results in a more hydrophobic mutant, whereas the substitutions Val→Phe and Val→Met reduce Aβ hydrophobicity. If increasing hydrophobicity stabilizes the fibril state, then one would expect ΔG_{fib} to be ordered as $\Delta G_{fib}(Ile) < \Delta G_{fib}(Val) < \Delta G_{fib}(Phe) < \Delta G_{fib}(Met)$. However, the opposite trend is observed, in which $\Delta G_{fib}(Ile) > \Delta G_{fib}(Val) > \Delta G_{fib}(Phe)$. The observed behavior of ΔG_{fib} is consistent with our results, which suggest that side-chain interactions may impede the formation of the locked fibrillike state. Therefore, we propose that the impact of side-chain interactions on the energetics of fibril growth is nonmonotonic. Moderate reduction in the strength of side-chain interactions may stabilize fibrillike states (such as locked), as seen in Figs. 5 *a* and 6. However, complete elimination of hydrophobic side chain, say, by Gly substitution, is expected to impede fibril growth (Fig. 6).

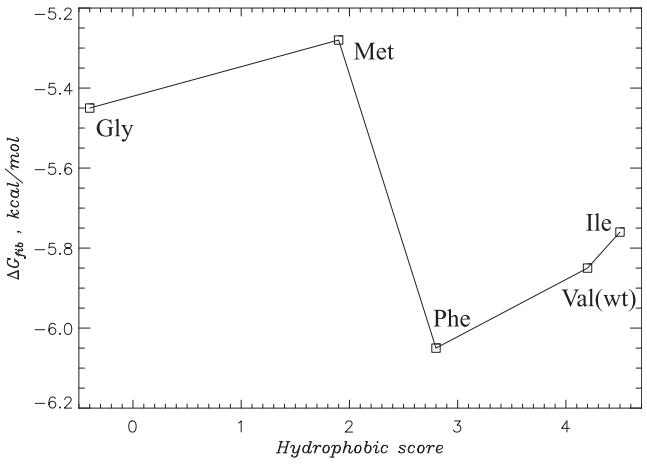

FIGURE 6 The experimental free energies of fibrillation ΔG_{fib} obtained for $A\beta_{1-40}$ peptide and its $Val^{18}X$ mutants as a function of Kyte-Doolittle hydrophobic score of the amino acid X. The amino acids next to the datapoints indicate the substitutions X.

To check these arguments in silico, we performed REMD simulations of two single-site Aβ mutants, $Phe^{19}Gly$ and $Phe^{19}Leu$, in which hydrophobic Phe is either deleted (Gly) or substituted with a less hydrophobic residue (Leu). For $Phe^{19}Gly$, the free energy gap between docked and locked states is reduced by 25% due to the higher free energy of the locked state. Simultaneously, the number of peptide-fibril pHBs $\langle N_{phb} \rangle$ decreases from 6.0 to 5.1. An opposite trend holds for $Phe^{19}Leu$, for which the free energy gap increases by 36% and $\langle N_{phb} \rangle$ reaches 6.6. These data are consistent with the experimental findings in Fig. 6 and with our prediction on the role of hydrophobic interactions in fibril growth, as stated above.

Finally, it is of interest to discuss our results in the context of recent experimental studies of Mukherjee et al. (60). These authors investigated Aβ aggregation in reverse micelles, in which a limited number of free water molecules (compared with the bulk) are available for peptide hydration. It is possible that the increase in aggregation rates observed upon encapsulation into reverse micelles is due to the reduction in the strength of hydrophobic interactions. In this case, the findings of Mukherjee et al. would be consistent with our data, suggesting that strong nonspecific hydrophobic interactions impede fibril growth.

CONCLUSIONS

Using REMD simulations, we probed the energetics of Aβ fibril elongation. Two conclusions follow from our results.

First, there are considerable variations in binding propensities along Aβ sequence. The peptides incorporated within the fibril and those binding to the fibril edge interact primarily through their N-termini. Therefore, the mutations affecting the Aβ positions 10–23 are expected to have the largest impact on fibril elongation compared with those occurring in the C-terminus and turn.

Second, by performing weak perturbations in binding free energy landscape, we proposed that strong side-chain interactions, in particular, hydrophobic contacts, impede fibril growth. Therefore, fibril elongation may be promoted by moderate reduction of Aβ hydrophobicity. However, complete elimination of hydrophobic residues is expected to hinder fibril growth.

SUPPORTING MATERIAL

Two equations, two figures, and two tables are available at http://www.biophysj.org/biophysj/supplemental/S0006-3495(09)00698-5.

The content is solely the responsibility of the authors and does not necessarily represent the official views of the National Institute on Aging or the

National Institutes of Health. Fig. 1 *a* was produced using the University of California at San Francisco Chimera package from the Resource for Biocomputing, Visualization, and Informatics at the University of California at San Francisco. The authors declare no competing financial interests.

This work was supported by grant No. R01 AG028191 from the National Institute on Aging (National Institutes of Health).

REFERENCES

1. Selkoe, D. J. 2003. Folding proteins in fatal ways. *Nature*. 426:900–904.
2. Dobson, C. M. 2003. Protein folding and misfolding. *Nature*. 426:884–890.
3. Shankar, G. M., S. Li, T. H. Mehta, A. Garcia-Munoz, N. E. Shepardson, et al. 2008. Amyloid-β protein dimers isolated directly from Alzheimers brains impair synaptic plasticity and memory. *Nat. Med.* 14:837–842.
4. Kayed, R., E. Head, J. L. Thompson, T. M. McIntire, S. C. Milton, et al. 2003. Common structure of soluble amyloid oligomers implies common mechanism of pathogenesis. *Science*. 300:486–489.
5. Haass, C., and D. J. Selkoe. 2007. Soluble protein oligomers in neurodegeneration: lessons from the Alzheimers amyloid β-peptide. *Nat. Rev. Mol. Cell Biol.* 8:101–112.
6. Pastor, M. T., N. Kammerer, V. Schubert, A. Esteras-Chopo, C. G. Dotti, et al. 2008. Amyloid toxicity is independent of polypeptide sequence, length and chirality. *J. Mol. Biol.* 375:695–707.
7. Murphy, R. M., and M. M. Pallitto. 2000. Probing the kinetics of β-amyloid self-association. *J. Struct. Biol.* 130:109–122.
8. Carulla, N., G. L. Caddy, D. R. Hall, J. Zurdo, M. Gair, et al. 2005. Molecular recycling within amyloid fibrils. *Nature*. 436:554–558.
9. Martins, I. C., I. Kuperstein, H. Wilkinson, E. Maes, M. Vanbrabant, et al. 2008. Lipids revert inert Aβ amyloid fibrils to neurotoxic protofibrils that affect learning in mice. *EMBO J.* 27:224–233.
10. Yoshiike, Y., T. Akagi, and A. Takashima. 2007. Surface structure of amyloid-β fibrils contributes to cytotoxicity. *Biochemistry*. 46:9805–9812.
11. Serpell, L. C. 2000. Alzheimer's amyloid fibrils: structure and assembly. *Biochim. Biophys. Acta*. 1502:16–30.
12. Burkoth, T. S., T. Benzinger, V. Urban, D. M. Morgan, D. M. Gregory, et al. 2000. Structure of the β-amyloid(10–35) fibril. *J. Am. Chem. Soc.* 122:7883–7889.
13. Petkova, A. T., W.-M. Yau, and R. Tycko. 2006. Experimental constraints on quaternary structure in Alzheimer's β-amyloid fibrils. *Biochemistry*. 45:498–512.
14. Luhrs, T., C. Ritter, M. Adrian, D. R. Loher, B. Bohrmann, et al. 2005. 3D structure of Alzheimers amyloid-β(1–42) fibrils. *Proc. Natl. Acad. Sci. USA*. 102:17342–17347.
15. Nelson, R., M. R. Sawaya, M. Balbirnie, A. O. Madsen, C. Riekel, et al. 2005. Structure of the cross-β spine of amyloid-like fibrils. *Nature*. 435:773–778.
16. Meersman, F., and C. M. Dobson. 2006. Probing the pressure-temperature stability of amyloid fibrils provides new insights into their molecular properties. *Biochim. Biophys. Acta*. 1764:452–460.
17. Murthy, R. M. 2002. Peptide aggregation in neurodegenerative disease. *Annu. Rev. Biomed. Eng*. 4:155–174.
18. Kirkitadze, M. D., G. Bitan, and D. B. Teplow. 2002. Paradigm shifts in Alzheimer's disease and other neurogenerative disorders: the emerging role of oligomeric assemblies. *J. Neurosci. Res.* 69:567–577.
19. Tseng, B. P., W. P. Esler, C. B. Clish, E. R. Stimson, J. R. Ghilardi, et al. 1999. Deposition of monomeric, not oligomeric, Aβ mediates growth of Alzheimers disease amyloid plaques in human brain preparations. *Biochemistry*. 38:10424–10431.
20. Esler, W. P., E. R. Stimson, J. M. Jennings, H. V. Vinters, J. R. Ghilardi, et al. 2000. Alzheimer's disease amyloid propagation by a template-dependent dock-lock mechanism. *Biochemistry*. 39:6288–6295.
21. Cannon, M. J., A. D. Williams, R. Wetzel, and D. G. Myszka. 2004. Kinetic analysis of β(-amyloid fibril elongation. *Anal. Biochem.* 328:67–75.
22. O'Nuallain, B., S. Shivaprasad, I. Kheterpal, and R. Wetzel. 2005. Thermodynamics of Aβ(1–40) amyloid fibril elongation. *Biochemistry*. 44:12709–12718.
23. Pawar, A. P., K. F. Dubay, J. Zurdo, F. Chiti, M. Vendruscolo, et al. 2005. Predictions of aggregation-prone and aggregation-susceptible regions in proteins associated with neurodegenerative diseases. *J. Mol. Biol.* 350:379–392.
24. Tartaglia, G., A. Cavalli, P. Pellarin, and A. Caflisch. 2005. Prediction of aggregation rate and aggregation-prone segments in polypeptide sequences. *Protein Sci.* 14:2723–2734.
25. Ma, B., and R. Nussinov. 2006. Simulations as analytical tools to understand protein aggregation and predict amyloid conformation. *Curr. Opin. Struct. Biol.* 10:445–452.
26. Ma, B., and R. Nussinov. 2002. Molecular dynamics simulations of alanine rich β-sheet oligomers: insight into amyloid formation. *Protein Sci.* 11:2335–2350.
27. Wu, C., H. Lei, and Y. Duan. 2005. Elongation of ordered peptide aggregate of an amyloidogenic hexapeptide NFGAIL observed in molecular dynamics simulations with explicit solvent. *J. Am. Chem. Soc.* 127:13530–13537.
28. Nguyen, P. H., M. S. Li, G. Stock, J. E. Straub, and D. Thirumalai. 2007. Monomer adds to preformed structured oligomers of Aβ-peptides by a two-stage dock-lock mechanism. *Proc. Natl. Acad. Sci. USA*. 104:111–116.
29. Krone, M. G., L. Hua, P. Soto, R. Zhou, B. J. Berne, et al. 2008. Role of water in mediating the assembly of Alzheimer amyloid-beta Aβ16–22 protofilaments. *J. Am. Chem. Soc.* 10.1021/ja8017303.
30. Takeda, T., and D. K. Klimov. 2008. Temperature-induced dissociation of Aβ monomers from amyloid fibril. *Biophys. J.* 95:1758–1772.
31. Takeda, T., and D. K. Klimov. 2009. Replica exchange simulations of the thermodynamics of Aβ fibril growth. *Biophys. J.* 96:442–452.
32. Ban, T., M. Hoshino, S. Takahashi, D. Hamada, K. Hasegawa, et al. 2004. Direct observation of Aβ amyloid fibril growth and inhibition. *J. Mol. Biol.* 344:757–767.
33. Sugita, Y., and Y. Okamoto. 1999. Replica-exchange molecular dynamics method for protein folding. *Chem. Phys. Lett.* 114:141–151.
34. Brooks, B. R., R. E. Bruccoleri, B. D. Olafson, D. J. States, S. Swaminathan, et al. 1982. CHARMM: a program for macromolecular energy, minimization, and dynamics calculations. *J. Comput. Chem.* 4:187–217.
35. Ferrara, P., J. Apostolakis, and A. Caflisch. 2002. Evaluation of a fast implicit solvent model for molecular dynamics simulations. *Proteins Struct. Funct. Bioinform.* 46:24–33.
36. Cecchini, M., F. Rao, M. Seeber, and A. Caflisch. 2004. Replica exchange molecular dynamics simulations of amyloid peptide aggregation. *J. Chem. Phys.* 121:10748–10756.
37. Garcia, A. E., and J. N. Onuchic. 2003. Folding a protein in a computer: an atomic description of the folding/unfolding of protein A. *Proc. Natl. Acad. Sci. USA*. 100:13893–13898.
38. Tsai, H.-H., M. Reches, C.-J. Tsai, K. Gunasekaran, E. Gazit, et al. 2005. Energy landscape of amyloidogenic peptide oligomerization by parallel-tempering molecular dynamics simulation: significant role of Asn ladder. *Proc. Natl. Acad. Sci. USA*. 102:8174–8179.
39. Baumketner, A., and J.-E. Shea. 2006. Folding landscapes of the Alzheimer amyloid-β(12–28) peptide. *J. Mol. Biol.* 362:567–579.
40. Jang, S., and S. Shin. 2008. Computational study on the structural diversity of amyloid beta peptide (Aβ10–35) oligomers. *J. Phys. Chem. B*. 112:3479–3484.
41. Klimov, D. K., and D. Thirumalai. 2003. Dissecting the assembly of $A\beta_{16-22}$ amyloid peptides into antiparallel β-sheets. *Structure*. 11: 295–307.
42. Kabsch, W., and C. Sander. 1983. Dictionary of protein secondary structure: pattern recognition of hydrogen-bonded and geometrical features. *Biopolymers*. 22:2577–2637.

43. Ferrenberg, A. M., and R. H. Swendsen. 1989. Optimized Monte Carlo data analysis. *Phys. Rev. Lett.* 63:1195–1198.

44. Shea, J. E., Y. D. Nochomovitz, Z. Guo, and C. L. Brooks. 1998. Exploring the space of protein folding Hamiltonians: the balance of forces in a minimalist β-barrel model. *J. Chem. Phys.* 109:2895–2903.

45. Fawzi, N. L., Y. Okabe, E.-H. Yap, and T. Head-Gordon. 2007. Determining the critical nucleus and mechanism of fibril elongation of the Alzheimer s $A\beta_{1-40}$ peptide. *J. Mol. Biol.* 365:535–550.

46. Yan, Y., and C. Wang. 2006. Aβ42 is more rigid than Aβ40 at the C terminus: implications for Aβ aggregation and toxicity. *J. Mol. Biol.* 364:853–862.

47. Sgourakis, N. G., Y. Yan, S. A. McCallum, C. Wang, and A. E. Garcia. 2007. The Alzheimers peptides Aβ40 and 42 adopt distinct conformations in water: a combined MD/NMR study. *J. Mol. Biol.* 368:1448–1457.

48. Hung, L. W., G. D. Ciccotosto, E. Giannakis, D. J. Tew, K. Perez, et al. 2008. Amyloid-β peptide (Aβ) neurotoxicity is modulated by the rate of peptide aggregation: Aβ dimers and trimers correlate with neurotoxicity. *J. Neurosci.* 28:11950–11958.

49. Hou, L., H. Shao, Y. Zhang, H. Li, N. K. Menon, et al. 2004. Solution NMR studies of the Aβ(1–40) and Aβ(1–42) peptides establish that the Met^{35} oxidation state affects the mechanism of amyloid formation. *J. Am. Chem. Soc.* 126:1992–2005.

50. Melquiond, A., X. Dong, N. Mousseau, and P. Derreumaux. 2008. Role of the region 23–28 in Aβ fibril formation: insights from simulations of the monomers and dimers of Alzheimer's peptides Aβ40 and Aβ42. *Curr. Alzh. Res.* 5:244–250.

51. Tjernberg, L. O., D. J. E. Callaway, A. Tjernbergi, S. Hahne, C. Lilliehoo, et al. 1999. A molecular model of Alzheimer amyloidβ-peptide fibril formation. *J. Biol. Chem.* 274:12619–12625.

52. Kirschner, D. A., H. Inouye, L. K. Duffy, A. Sinclair, M. Lind, et al. 1987. Synthetic peptide homologous to β protein from Alzheimer disease forms amyloid-like fibrils in vitro. *Proc. Natl. Acad. Sci. USA.* 84:6953–6957.

53. Wurth, C., N. K. Guimard, and M. H. Hecht. 2002. Mutations that reduce aggregation of the Alzheimers Aβ42 Peptide: an unbiased search for the sequence determinants of Aβ amyloidogenesis. *J. Mol. Biol.* 319:1279–1290.

54. de Groot, N. S., F. X. Aviles, J. Vendrell, and S. Ventura. 2006. Mutagenesis of the central hydrophobic cluster in Aβ42 Alzheimer's peptide. *FEBS J.* 273:658–668.

55. Lu, Y., P. Derreumaux, Z. Guo, N. Mousseau, and G. Wei. 2008. Thermodynamics and dynamics of amyloid peptide oligomerization are sequence dependent. *Proteins Struct. Funct. Bioinform.* 75:954–963.

56. Esler, W. P., E. R. Stimson, J. R. Ghilardi, Y.-A. Lu, A. M. Felix, et al. 1996. Point substitution in the central hydrophobic cluster of a human β-amyloid congener disrupts peptide folding and abolishes plaque competence. *Biochemistry.* 35:13914–13921.

57. Meinhardt, J., G. G. Tartaglia, A. Pawar, T. Christopeid, P. Hortschansky, et al. 2007. Similarities in the thermodynamics and kinetics of aggregation of disease-related Aβ(1–40) peptides. *Protein Sci.* 16:1214–1222.

58. Bieschke, J., Q. Zhang, E. T. Powers, R. A. Lerner, and J. W. Kelly. 2005. Oxidative metabolites accelerate Alzheimers amyloidogenesis by a two-step mechanism, eliminating the requirement for nucleation. *Biochemistry.* 44:4977–4983.

59. Peim, A., P. Hortschansky, T. Christopeid, V. Schroeckh, W. Richter, et al. 2006. Mutagenic exploration of the cross-seeding and fibrillation propensity of Alzheimers β-amyloid peptide variants. *Protein Sci.* 15:1801–1805.

60. Mukherjee, S., P. Chowdhury, and F. Gai. 2009. Effect of dehydration on the aggregation kinetics of two amyloid peptides. *J. Phys. Chem. B.* 113:531–535.

61. Pettersen, E. F., T. D. Goddard, C. C. Huang, G. S. Couch, D. M. Greenblatt, et al. 2004. UCSF Chimera—a visualization system for exploratory research and analysis. *J. Comput. Chem.* 25:1605–1612.